

Electronic Coherence and Coherent Dephasing in the Optical Control of Electrons in Graphene

Christian Heide,^{*,||} Timo Eckstein,^{||} Tobias Boolakee, Constanze Gerner, Heiko B. Weber, Ignacio Franco, and Peter Hommelhoff



Cite This: *Nano Lett.* 2021, 21, 9403–9409



Read Online

ACCESS |



Metrics & More



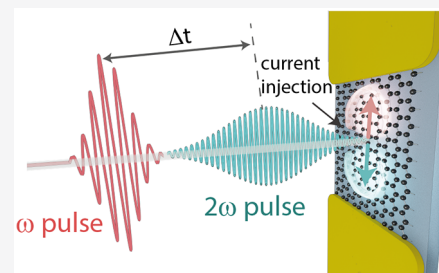
Article Recommendations



Supporting Information

ABSTRACT: Electronic coherence is of utmost importance for the access and control of quantum-mechanical solid-state properties. Using a purely electronic observable, the photocurrent, we measure a lower bound of the electronic coherence time of 22 ± 4 fs in graphene. The photocurrent is ideally suited to measure electronic coherence, as it is a direct result of coherent quantum-path interference, controlled by the delay between two ultrashort two-color laser pulses. The maximum delay for which interference between the population amplitude injected by the first pulse interferes with that generated by the second pulse determines the electronic coherence time. In particular, numerical simulations reveal that the experimental data yields a lower bound on the electronic coherence time, masked by coherent dephasing due to the broadband absorption in graphene. We expect that our results will significantly advance the understanding of coherent quantum control in solid-state systems ranging from excitation with weak fields to strongly driven systems.

KEYWORDS: *electronic coherence, coherent control, two-color excitation, graphene, coherent dephasing, light–matter interaction*



Within the last 25 years, the role of electronic coherence in solid-state systems has been pivotal in ultrafast optoelectronics.^{1–6} Several experimental schemes have been applied to study the underlying lifetime of coherence, which can range from picoseconds in cold atoms^{7,8} down to single femtoseconds in highly excited semiconductors and metals.^{1,9} One key to measure coherence is the access to an interference process, such as used in coherent spectroscopy^{4,9,10} or four-wave mixing.¹¹ As a counterpart to these experiments relying on optical polarization or nonlinear photoemission spectroscopy,^{10,12–15} we will show that a residual current, which is a direct result of quantum-path interference in solids, can serve as an ideal observable to measure electronic coherence in solids. While there are various measurements demonstrating the coherent control in solids,^{16–21} the underlying time scale of electronic coherence is mostly obscured due to the lack of ultrafast pulses. Furthermore, when short laser pulses and thus broadband resonant excitations are used, coherent dephasing, also known as inhomogeneous broadening, masks the current signal for large temporal delays.²² We discuss this effect in the context of Figure 3.

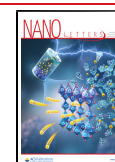
Figure 1a shows schematically the experimental setup to measure a coherently injected residual current using two ultrashort laser pulses, one oscillating at frequency ω (≈ 800 nm, red pulse) and one at 2ω (≈ 400 nm, blue pulse). In particular, light of low temporal symmetry can generate net currents in solids, even in the absence of a bias voltage or spatial asymmetries in the material.^{5,16–18,20,23–27} In the perturbative limit, such light-induced symmetry breaking arises

by the interference of an even- and odd-order pathway from a given initial to a final momentum state, as schematically shown in Figure 1b for one- versus two-photon absorption.^{16–19,28,29} By changing the relative phase via the temporal delay between the two colors, the quantum interference and thus the net current amplitude and direction can be controlled. Intriguingly, this interference process persists beyond the perturbative regime and expands to the strong-field regime. In the strong-field limit the wavenumber of electrons significantly changes with the laser electric field, i.e., $dk(t)/dt \propto E(t)$, which gives rise to coupled intraband electron dynamics and interband transitions. Depending on the symmetry of the applied laser field, the interference between intra- and interband light-induced electron dynamics, so-called Landau–Zener–Stückelberg interference, leads to a phase-controllable net current.^{5,30–32} While for low field strengths and long laser pulses the latter can be neglected, it becomes important for strong and few-cycle laser pulses. Generally, in all these regimes, i.e., weak or strong excitation, the residual current generation process requires electronic coherence to emerge, as it relies on interference.³³ Scattering with phonons is a source of decoherence, leading to a suppression of the light-injected

Received: June 29, 2021

Revised: October 14, 2021

Published: November 4, 2021



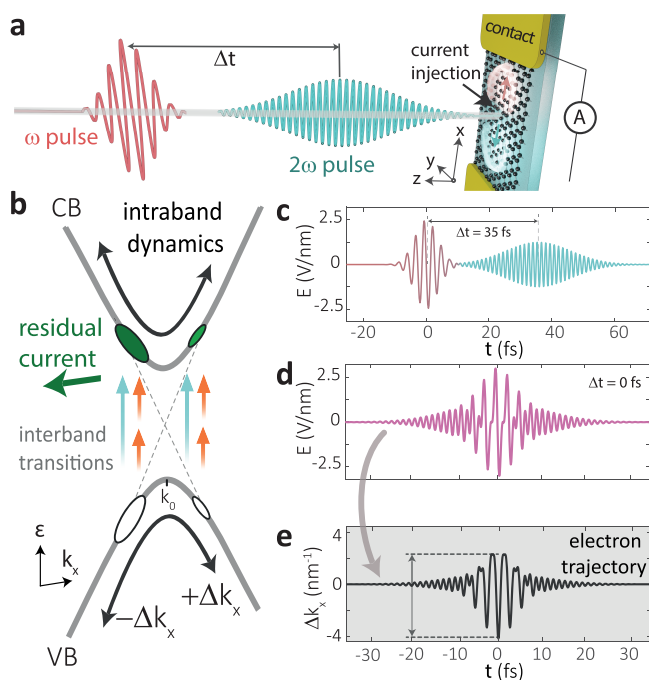


Figure 1. Residual current generation using $\omega + 2\omega$ two-color laser fields. (a) Experimental scheme. The x -polarized two-color laser field injects a directional residual current in the x -direction, which is probed with two metal electrodes. (b) Schematic illustration of two-color quantum-path interference near the band gap. The interference of one- vs two-photon excitation generates a phase-dependent asymmetry in the electron and hole population distributions, giving rise to a residual current. (c, d) Electric field waveform of a 6 fs few-cycle laser pulse and its second harmonic with a pulse duration of 19 fs for a temporal delay of $\Delta t = 35$ fs (c) and $\Delta t = 0$ (d). (e) Light-induced electron dynamics for $\Delta t = 0$ [case (d)] exhibits a clear negative peak in momentum space (k -space), breaking the inversion symmetry of graphene [black arrows in (b)].

current, as the electrons lose their ability to interfere.^{1,9,34,35} Whereas the current is a purely electronic observable arising from electron interference, commonly applied methods to measure coherence, based on the optical response of matter, rely on measuring the optical polarization. While such measurements offer information about coherence between optically active states, it is often hard to disentangle electronic and vibrational contributions to the resulting signal, making it challenging to directly measure electronic coherence.^{9,36–38}

In this Letter, we demonstrate the ability to monitor electronic coherence by injecting a two-color photocurrent in graphene, using the scheme shown in Figure 1a. The combined two-color laser field is described as $E(t) = E_{\omega}(t) \cos(\omega t + \varphi_{\omega}) + E_{2\omega}(t + \Delta t) \cos(2\omega(t + \Delta t) + \varphi_{2\omega})$, with Δt the delay between both pulses and $E_{\omega}(t)$ and $E_{2\omega}(t + \Delta t)$ the envelope functions of the laser pulses with angular frequencies of ω and 2ω , respectively. Figure 1c,d shows the combined electric fields for a temporal delay of $\Delta t = 35$ fs and $\Delta t = 0$. From $E(t)$, the corresponding electron trajectory in the reciprocal space is obtained by the Bloch acceleration theorem $dk(t)/dt = \hbar^{-1}eE(t)$ (Figure 1e). We have previously demonstrated that such an asymmetric electron trajectory results in the injection of a residual current, which can be interpreted on the basis of Landau–Zener–Stückelberg interference.^{5,39} To the lowest order, the net DC current density j emerges as a third-order process in the photoresponse^{16–18,25,33}

$$j \propto E_{0,2\omega} E_{0,\omega}^2 \sin(2\varphi_{\omega} - \varphi_{2\omega} - 2\omega\Delta t) \quad (1)$$

where $E_{0,\omega}$ and $E_{0,2\omega}$ are the peak electric field strengths. The dependence of the relative phase on the time delay between the two colors is given by $\varphi_{\text{Delay}}(\Delta t, \omega) = 2\omega\Delta t$.^{16,17,29} The formalism that leads to eq 1 requires continuous wave excitation, where only excitations separated by $2\hbar\omega$ contribute to the phase-controllable residual current (see blue and red arrows in Figure 1b). In other words, the asymmetry of the excitations probability can be understood by considering the k -dependence of the interband momentum matrix elements, which can be out of phase for electrons at $k_x < 0$ and $k_x > 0$.¹⁹ Thus, if the interference at $k_x < 0$ is constructive, resulting in net population transfer from the valence (VB) to the conduction band (CB), the interference at $k_x > 0$ is destructive (no population). This imbalance in the population distribution creates a net phase-controllable residual current. In the context of pulsed excitation (broad optical spectrum), this refers to a broader set of energy levels that are excited. In contrast, when strong laser pulses are applied, intraband motion may become important and different spectral components cannot be treated independently, which are beyond eq 1. We will discuss the latter case in Figure 3, on the basis of numerical simulations.

In the experiment, we focus a few-cycle fundamental and a frequency-doubled femtosecond laser field to the center of a $10 \times 2 \mu\text{m}^2$ graphene strip, as depicted in Figure 1a. The monolayer graphene is epitaxially grown on silicon carbide (4H-SiC) and connected to two electrodes.⁵ The focal radii are $1.9 \pm 0.1 \mu\text{m}$ ($1/e^2$ intensity) for both the ω and 2ω pulses, and thus, the electrodes are hardly illuminated by the laser field. The sample is placed under vacuum ($\sim 10^{-6}$ hPa). Laser pulses from an 80 MHz Ti:sapphire laser oscillator with a center wavelength of 800 nm are frequency-doubled using a β -barium borate (BBO) crystal. Both colors are separately controlled in a two-color interferometer and sent to the sample. This setup allows independent control of the relative phase, intensity, polarization, and dispersion. The resulting pulse duration of $\tau_{\omega} = 6.0 \pm 0.5$ fs [intensity full width at half-maximum (fwhm)] for the fundamental is measured via spectral phase interferometry for direct electric-field reconstruction (SPIDER), while its second harmonic with a pulse duration of $\tau_{2\omega} = 19 \pm 2$ fs (17 fs Fourier limit) is determined via a cross-correlation frequency-resolved optical gating (XFROG). We note that both pulses do not spectrally overlap, and thus, optical interference between both pulses does not occur. We perform a lock-in measurement referenced to a periodic modulation of the temporal delay between both colors to isolate the relative phase-dependent current as given by eq 1. For further noise suppression, we apply post-processing filters to eliminate high-frequency noise and DC contributions, which may occur due to sample imperfections.⁴⁰

Figure 2a shows the measured phase-dependent current as a function of the temporal delay Δt . The applied peak electric field strengths are $E_{0,\omega} = 2.1$ V/nm and $E_{0,2\omega} = 0.3$ V/nm, resulting in a maximum $\omega + 2\omega$ current of 5 nA. The central region of the overlap scan is magnified in Figure 2b. Changing the temporal delay Δt by a fourth of the 2ω -period, i.e., by $T_{2\omega}/4 = 0.34$ fs, results in a fully symmetric electron trajectory and, thus, no current is measured. Delaying the two pulses by $T_{2\omega}/2 = 0.68$ fs reverses the current direction. The amplitude of the Fourier transform over the entire phase-sensitive current signal, shown in Figure 2c, exhibits a clear peak at $2\omega = 2\pi \times 750$ THz ($800 \text{ nm} \hat{=} 375$ THz), as also expected from eq 1.

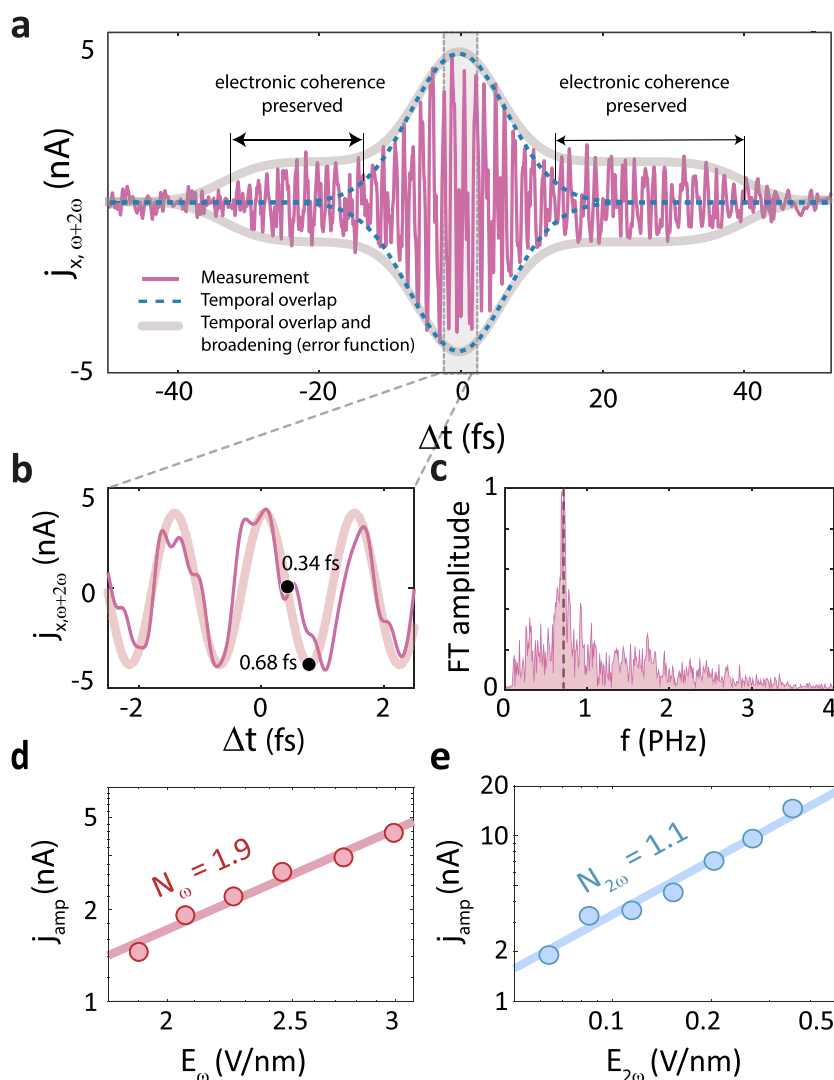


Figure 2. Coherent $\omega + 2\omega$ phase-controlled current generation in graphene. (a) Measured current as a function of temporal delay Δt . $\Delta t < 0$ means that the 2ω pulse arrives before the ω pulse. The field strengths are $E_{0,\omega} = 2.1$ V/nm and $E_{0,2\omega} = 0.3$ V/nm. The maximum current is observed when both pulses are in temporal overlap. The blue dashed lines mark the main temporal overlap region of the laser pulses. Note that for a coherence time shorter than the pulse durations, a coherent signal can only be observed within the blue dashed envelope. The gray lines enclose delays beyond the temporal overlap of the pulses, hence, electronic coherence is required to form this current via two-color interference. (b) Magnification of the central area of (a). A sine function with a frequency of 2ω ($2\pi \times 750$ THz) is shown as a thick light line. (c) Fourier transform (FT) amplitude of the data in (a). The current consists almost exclusively of an oscillatory component at 2ω . (d, e) Amplitude of the $\omega + 2\omega$ current as a function of $E_{0,\omega}$ and $E_{0,2\omega}$. (d) $E_{0,\omega}$ was varied between 1.9 and 3.0 V/nm, while $E_{0,2\omega}$ was fixed to 0.07 V/nm. (e) $E_{0,2\omega}$ takes values between 0.06 and 0.42 V/nm, with $E_{0,\omega}$ fixed to 2.1 V/nm. The solid lines are linear fits of the double-logarithmic representation, indicating the perturbative orders of the response: ≈ 2 for the variation of $E_{0,\omega}$ and ≈ 1 for $E_{0,2\omega}$ as expected.

Additionally, we determine the scaling of the maximal current amplitude j_{amp} as a function of $E_{0,\omega}$ and $E_{0,2\omega}$. We observe a power-law scaling with nonlinearities of $N_{\omega} = 1.86 \pm 0.15$ and $N_{2\omega} = 1.09 \pm 0.10$ for the variation of $E_{0,\omega}$ and $E_{0,2\omega}$ respectively (Figure 2d,e), which is also supported by eq 1. Hence, the periodicity of the current modulation as a function of the delay and the power-law scaling corroborate the $\omega + 2\omega$ excitation scheme even in the presence of broadband excitation and high electric field strengths.

The entire signal shown in Figure 2a consists of two regimes. The inner part resembles a Gaussian distribution with a width of 17 fs (fwhm, blue dashed line). Furthermore, there is an asymmetric outer part with a broadening of the signal up to -32 fs for negative delay (2ω arrives first) and 39 fs for positive delay (ω arrives first). To obtain these values, we fit a

Gaussian envelope with two error functions, shown as a gray line. Importantly, the signal outside the main temporal overlap region, indicated by the blue dashed line, is used in the following to determine the electronic coherence time.

To understand the role of electronic coherence in the current generation process more quantitatively, we model the electron dynamics in graphene using a nearest-neighbor tight-binding model with minimal coupling of the laser field for the applied laser parameters.^{5,41,42} The residual conduction band population is obtained by numerically integrating the time-dependent Schrödinger equation (TDSE). In the simulation, we use a carrier-envelope phase of zero for the fundamental to avoid current generation due to the low temporal symmetry of the fundamental pulse.⁵ Thus, all currents obtained in the following are of two-color nature.

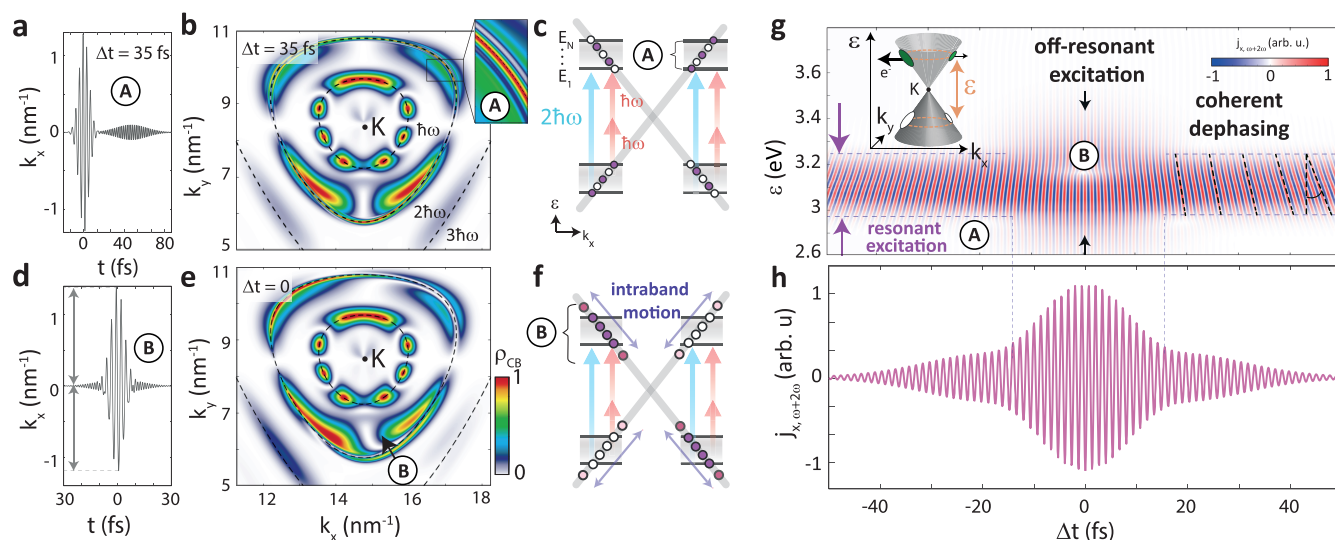


Figure 3. Numerical simulation results of two-color excitation in graphene. (a) Electron trajectory $k_x(t)$ for $\Delta t = 35$ fs, when both pulses barely overlap in time. (b) TDSE results of $\rho_{CB}(k)$ around the K-point after excitation with the two-color laser field ($\Delta t = 35$ fs). $\rho_{CB} = 1$ means that the entire population is transferred from the valence to the conduction band. The dashed lines indicate multiphoton resonances, where the energy difference of VB and CB corresponds to the photon energies $\hbar\omega$, $2\hbar\omega$, and $3\hbar\omega$. (c) Schematic illustration of the current excitation process. Although separated in time, one-photon absorption with a photon energy of $2\hbar\omega$ and two-photon absorption with a photon energy of $\hbar\omega$ may interfere, governing ρ_{CB} . Due to the broadband optical spectrum of the applied laser fields, a set of energy levels is involved in the photocurrent. Each level accumulates a phase given by $2\omega\Delta t$. Averaging over this ensemble of contributions leads to coherent dephasing of the photocurrent. This effect is also known as inhomogeneous broadening. (d–f) Panels for $\Delta t = 0$ fs. The two arrows in (d) indicate the asymmetry between maximum positive and negative k_x . We note that this asymmetry is absent in (a), as $\Delta t = 0$. (g) Energy-dependent current as a function of Δt . For $|\Delta t| > 17$ fs, excitation is found resonantly only at $2\hbar\omega$, with a width given by the spectral width of the laser fields. With the increasing delay and thus, increasing spectral phase, the populations at different excitation energies are increasingly out of phase causing coherent dephasing in the (energy-integrated) residual current [see (h)]. When both pulses temporally overlap, additional symmetry breaking, caused by intraband motion results in off-resonant current contributions. (h) Total current, as a function of Δt .

We discuss the simulation results of the delay-dependent current in two parts: (A) when both pulses do *not* temporally overlap and (B) when both pulses do temporally overlap. These cases are marked with circled labels A and B throughout Figure 3. In Figure 3a (case A) both pulses are temporally separated by $\Delta t = 35$ fs and thus hardly overlap in time. Figure 3b shows the corresponding numerically obtained residual conduction band (CB) population ρ_{CB} close to the K-point. Around the K-point resonant one-photon and two-photon absorption of the ω pulse can be found. Additionally, one-photon absorption of the 2ω pulse excites carriers to the conduction band. In the spectral overlap region of the two colors, i.e., at the $2\hbar\omega$ resonance line, ρ_{CB} is manipulated by the relative phase between the two absorption pathways (see inset of Figure 3b, red and blue arrows in Figure 3c). A population imbalance between k -states on the left and right sides of the K-points results in a net current. For $\Delta t = 0$, all resonantly excited k -states experience the same spectral phase. Increasing Δt introduces an additional spectral phase $\varphi_{\text{Delay}}(\Delta t, \omega) = 2\omega\Delta t$ and, thus, a spectrally dependent phase at each k -point. As a result, the population distribution is modulated as a function of the spectral excitation energy, as shown in the numerical results (see the magnified area in Figure 3b) and schematically illustrated in Figure 3c with the filled and solid circles. Depending on the phase, the interference at each single k -point is either constructive, resulting in excitation, or destructive, resulting in no excitation.

Before we discuss this further, we note that in case B both pulses temporally overlap, as shown in Figure 3d. Here, electrons experience asymmetric trajectories (intraband motion), resulting in additional symmetry breaking and off-

resonant excitation (see Figure 3d longer electron trajectory for $k_x > 0$ and Figure 3f). As a result, Figure 3e reveals a strongly asymmetric resonant and off-resonant residual population distribution.^{30,39} While in principle the off-resonant population contributes to the current generation process, for the applied laser parameters, the resonant contribution at 2ω dominates, which also matches the power-law scaling observed in Figure 2d,e.

To understand how a residual current emerges, we first evaluate ρ_{CB} along constant energies between the valence and conduction bands $\varepsilon = \varepsilon_{CB} - \varepsilon_{VB}$ (see inset of Figure 3g, orange rings around the K-point). The current at $\varepsilon = 3.1$ eV corresponds to the energy of one-photon absorption of the 2ω pulse (1×3.1 eV) and two-photon absorption of the ω pulse (2×1.55 eV). In Figure 3g we plot the current as a function of energy ε for delays ranging from -50 to 50 fs. Finally, integrating over all energies results in the total residual current (Figure 3h). This current is maximized when both pulses are in temporal overlap and decreases as a function of delay.

On the basis of the simulation results, we are now able to discuss the roles of coherence, coherent dephasing, and off-resonant excitations in the delay-dependent current. When both pulses are temporally separated (case A), we see from Figure 3g that the two-color current originates from a resonant excitation at around 3.1 eV. Also in Figure 3g we see that the spectral phase introduced by the delay results in a shearing of the current modulation in the $\varepsilon - \Delta t$ plot (see dashed lines). Importantly, it is this shearing that leads to a reduction of the total current after integration (Figure 3h). This effect is known as coherent dephasing,⁴³ originating from the spectrally dependent phase $\varphi_{\text{Delay}}(\Delta t, \omega)$. Therefore, in the simulation

coherent dephasing reduces the integrated residual current, despite the coherence at a single k-point is preserved.

In contrast, when both pulses are in temporal overlap (case B) the current contributions are in phase and do not cancel out. Further, additional symmetry breaking due to the two-color laser field results in off-resonant excitation, which slightly influences the current amplitude. In [Video 1](#) (Supporting Information), we show the time evolution of the conduction band population. The video shows most clearly that in the overlap region B off-resonant excitation emerges. Yet, the main current contribution originates from the resonant excitation ([Figures 2d,e](#)).

We note that for the applied laser parameters, we are in a regime where the Rabi frequency at the two-photon resonance $\Omega_{R=VF}(E_{\omega,0}^2 + E_{2\omega,0})/(2\hbar\omega)^{-1} = 2\pi \times 123$ THz is high, but still smaller than $2\omega = 2\pi \times 750$ THz,^{5,39} with $v_F = 1$ nm/fs the Fermi velocity in graphene and e the elementary electric charge. Thus, non-resonant excitation might be expected, as discussed above for case B, but the dominating current contribution is expected to emerge from resonant excitation. These off-resonant excitations are naturally included in our TDSE model simulations. On the basis of the numerical simulations and the power-law scaling, shown in [Figure 2d](#), we have not observed significant deviations from perturbative $\omega + 2\omega$ coherent control. For higher electric field strengths, we may expect that the coherent control enters the strong-field regime.

The good agreement between experiment ([Figure 2a](#)) and simulation ([Figure 3h](#)) allows us to argue that electronic coherence is preserved at least up to 18 fs for the negative delay and 26 fs for the positive delay, given by the error functions (black arrows in [Figure 2a](#)). For larger delays, the signal is masked by coherent dephasing, causing the current to decay. To account for dephasing in the simulation, we implement a phenomenological dephasing time T_2 to our model simulations.⁴⁴ For T_2 shorter than the wings shown in [Figure 3h](#), the coherently broadened signal vanishes. [Video 2](#) in the Supporting Information shows the temporal evolution of the conduction band population and the resulting current trace with ($T_2 = 10$ fs). The temporal evolution without additional dephasing is shown in [Video 1](#). This comparison clearly supports that the temporal broadening of the current signal originates from the preserved electronic coherence. Whereas the experiment shows a shorter coherence time when the 2ω pulse arrives first, the simulation shows a symmetrical $\omega + 2\omega$ trace. One reason for this asymmetric behavior might be that for $\Delta t < 0$ the first pulse (2ω) generates the population via one-photon absorption, which could lead to a higher initial population and a population-dependent T_2 . While the current amplitude, which is the result of interference, is only sensitive to the overlap of the two populations, a possible initial population-dependent decoherence time might break the symmetry.¹ Time-dependent density functional theory simulations accounting for the critical role of decoherence and correlation effects are required, which are beyond the scope of this work.^{26,45} To determine the lower bound of the electronic coherence time, we take the mean of both values to obtain 22 ± 4 fs.

By comparing these decoherence times with a reported thermalization time of 50–80 fs in graphene, which involves multiple incoherent scattering events, we find that the here observed lower bound of the coherence time is about 2–3 times shorter.^{46–48}

The coherence time obtained from the photocurrent measurements reflects electronic coherence and coherent dephasing. While the latter reduces the current amplitude, it does not affect the electronic coherence. In coherent spectroscopy, such as in pulse echo experiments, these two dephasing channels are usually considered as T_2^* , reflecting both natural T_2 dephasing and dephasing caused by inhomogeneities in the ensemble.^{43,49–51} By introducing a frequency gradient to one of the pulses, T_2^* can be corrected for coherent dephasing. A similar approach might be possible here, namely by shaping the spectral phase of one of the laser pulses to correct for coherent dephasing. In such a scenario, the observed phase shift of the current as a function of energy, shown in [Figure 3g](#), can be compensated. Then, the photocurrent can directly be used to monitor electronic coherence.⁴³

In summary, we present a lower bound for the electronic coherence time in graphene of 22 ± 4 fs. To measure it, we use quantum-path interference and the resulting current, generated by a two-color laser field as an observable. The ultrafast nature of the laser pulses employed and the ability to time-delay them offer an ideal probe for monitoring this coherence. By shaping the spectral phase of the laser pulses, we propose the possibility of disentangling decoherence and coherent dephasing in a manner similar to pulse echo experiments. We expect that this versatile and efficient method for measuring electronic coherence based on a purely electronic observable will find widespread use in vastly different systems and experimental configurations.

■ ASSOCIATED CONTENT

Supporting Information

The Supporting Information is available free of charge at <https://pubs.acs.org/doi/10.1021/acs.nanolett.1c02538>.

Video 1: Temporal evolution of the conduction band population and resulting $\omega + 2\omega$ current without additional dephasing (AVI)

Video 2: Temporal evolution of the conduction band population and resulting $\omega + 2\omega$ current with additional dephasing ($T_2 = 10$ fs) (AVI)

■ AUTHOR INFORMATION

Corresponding Author

Christian Heide – Department of Physics, Friedrich-Alexander-Universität Erlangen-Nürnberg (FAU), D-91058 Erlangen, Germany; Stanford PULSE Institute, SLAC National Accelerator Laboratory, Menlo Park, California 94025, United States; orcid.org/0000-0002-7652-3241; Email: cheide@stanford.edu

Authors

Timo Eckstein – Department of Physics, Friedrich-Alexander-Universität Erlangen-Nürnberg (FAU), D-91058 Erlangen, Germany

Tobias Boolakee – Department of Physics, Friedrich-Alexander-Universität Erlangen-Nürnberg (FAU), D-91058 Erlangen, Germany

Constanze Gerner – Department of Physics, Friedrich-Alexander-Universität Erlangen-Nürnberg (FAU), D-91058 Erlangen, Germany

Heiko B. Weber – Department of Physics, Friedrich-Alexander-Universität Erlangen-Nürnberg (FAU), D-91058 Erlangen, Germany; orcid.org/0000-0002-6403-9022

Ignacio Franco – Departments of Chemistry and Physics, University of Rochester, Rochester, New York 14627, United States; orcid.org/0000-0002-0802-8185

Peter Hommelhoff – Department of Physics, Friedrich-Alexander-Universität Erlangen-Nürnberg (FAU), D-91058 Erlangen, Germany

Complete contact information is available at:
<https://pubs.acs.org/10.1021/acs.nanolett.1c02538>

Author Contributions

[†]C.H. and T.E. contributed equally.

Notes

The authors declare no competing financial interest.

ACKNOWLEDGMENTS

This work has been supported in part by the Deutsche Forschungsgemeinschaft (SFB 953 “Synthetic Carbon Allotropes”) and the PETACom project financed by Future and Emerging Technologies Open H2020 program. T.E. appreciates the support of the Friedrich Naumann Foundation for Freedom and the International Max Planck Research School Physics of Light. C.H. acknowledges support by the Alexander von Humboldt Foundation and the Max Planck School for Photonics. I.F. is supported by the National Science Foundation under Grant No. CHE-2102386.

REFERENCES

- (1) Bigot, J. Y.; Portella, M. T.; Schoenlein, R. W.; Cunningham, J. E.; Shank, C. V. Two-dimensional carrier-carrier screening in a quantum well. *Phys. Rev. Lett.* **1991**, *67*, 636–639.
- (2) Krausz, F.; Stockman, M. I. Stockman, “Attosecond metrology: from electron capture to future signal processing. *Nat. Photonics* **2014**, *8*, 205–213.
- (3) Hohenleutner, M.; Langer, F.; Schubert, O.; Knorr, M.; Huttner, U.; Koch, S. W.; Kira, M.; Huber, R. Real-time observation of interfering crystal electrons in high-harmonic generation. *Nature* **2015**, *523*, 572–575.
- (4) Cundiff, S. T. Coherent spectroscopy of semiconductors. *Opt. Express* **2008**, *16*, 4639–4664.
- (5) Higuchi, T.; Heide, C.; Ullmann, K.; Weber, H. B.; Hommelhoff, P. Light-field-driven currents in graphene. *Nature* **2017**, *550*, 224–228.
- (6) Reutzler, M.; Li, A.; Petek, H. Coherent Two-Dimensional Multiphoton Photoelectron Spectroscopy of Metal Surfaces. *Phys. Rev. X* **2019**, *9*, 011044.
- (7) Maunz, P.; Moehring, D. L.; Olmschenk, S.; Younge, K. C.; Matsukevich, D. N.; Monroe, C. Quantum interference of photon pairs from two remote trapped atomic ions. *Nat. Phys.* **2007**, *3*, 538–541.
- (8) Koch, C. P.; Shapiro, M. Coherent Control of Ultracold Photoassociation. *Chem. Rev.* **2012**, *112*, 4928.
- (9) Petek, H.; Ogawa, S. Femtosecond time-resolved two-photon photoemission studies of electron dynamics in metals. *Prog. Surf. Sci.* **1997**, *56*, 239–310.
- (10) Reutzler, M.; Li, A.; Wang, Z.; Petek, H. Coherent multidimensional photoelectron spectroscopy of ultrafast quasiparticle dressing by light. *Nat. Commun.* **2020**, *11*, 1–5.
- (11) Cundiff, S. T. Effects of correlation between inhomogeneously broadened transitions on quantum beats in transient four-wave mixing. *Phys. Rev. A: At., Mol., Opt. Phys.* **1994**, *49*, 3114–3118.
- (12) Petek, H.; Heberle, A. P.; Nessler, W.; Nagano, H.; Kubota, S.; Matsunami, S.; Moriya, N.; Ogawa, S. Optical phase control of

coherent electron dynamics in metals. *Phys. Rev. Lett.* **1997**, *79*, 4649–4652.

(13) Ogawa, S.; Nagano, H.; Petek, H.; Heberle, A. P. Optical dephasing in cu(111) measured by interferometric two-photon time-resolved photoemission. *Phys. Rev. Lett.* **1997**, *78*, 1339–1342.

(14) Gütde, J.; Rohleder, M.; Meier, T.; Koch, S. W.; Höfer, U. Coherently Controlled Electric. *Science* **2007**, *318*, 1287–1291.

(15) Tan, S.; Argondizzo, A.; Wang, C.; Cui, X.; Petek, H. Ultrafast multiphoton thermionic photoemission from graphite. *Phys. Rev. X* **2017**, *7*, 011004.

(16) Atanasov, R.; Haché, A.; Hughes, J. L. P.; Van Driel, H. M.; Sipe, J. E. Coherent Control of Photocurrent Generation in Bulk Semiconductors. *Phys. Rev. Lett.* **1996**, *76*, 1703–1706.

(17) Haché, A.; Kostoulas, Y.; Atanasov, R.; Hughes, J. L. P.; Sipe, J. E.; van Driel, H. M. Observation of coherently controlled photocurrent in unbiased, bulk GaAs. *Phys. Rev. Lett.* **1997**, *78*, 306–309.

(18) Dupont, E.; Corkum, P. B.; Liu, H. C.; Buchanan, M.; Wasilewski, Z. R. Phase-controlled currents in semiconductors. *Phys. Rev. Lett.* **1995**, *74*, 3596–3599.

(19) Fortier, T. M.; Roos, P. A.; Jones, D. J.; Cundiff, S. T.; Bhat, R. D. R.; Sipe, J. E. Carrier-envelope phase-controlled quantum interference of injected photocurrents in semiconductors. *Phys. Rev. Lett.* **2004**, *92*, 147403.

(20) Sun, D.; Divin, C.; Rioux, J.; Sipe, J. E.; Berger, C.; de Heer, W. A.; First, P. N.; Norris, T. B. Coherent control of ballistic photocurrents in multilayer epitaxial graphene using quantum interference. *Nano Lett.* **2010**, *10*, 1293–1296.

(21) Sun, D.; Divin, C.; Mihnev, M.; Winzer, T.; Malic, E.; Knorr, A.; Sipe, J. E.; Berger, C.; de Heer, W. A.; First, P. N.; Norris, T. B. Current relaxation due to hot carrier scattering in graphene. *New J. Phys.* **2012**, *14*, 105012.

(22) Weida, M. J.; Ogawa, S.; Nagano, H.; Petek, H. Ultrafast interferometric pump–probe correlation measurements in systems with broadened bands or continua. *J. Opt. Soc. Am. B* **2000**, *17*, 1443.

(23) Armstrong, J. A.; Bloembergen, N.; Ducuing, J.; Pershan, P. S. Interactions between light waves in a nonlinear dielectric. *Phys. Rev.* **1962**, *127*, 1918–1939.

(24) Garzon-Ramirez, A. J.; Franco, I. Stark control of electrons across interfaces. *Phys. Rev. B: Condens. Matter Mater. Phys.* **2018**, *98*, No. 121305(R).

(25) Garzon-Ramirez, A. J.; Franco, I. Symmetry breaking in the Stark Control of Electrons at Interfaces (SCELI). *J. Chem. Phys.* **2020**, *153*, 044704.

(26) Neufeld, O.; Tancogne-Dejean, N.; De Giovannini, U.; Hubener, H.; Rubio, A. Light-driven extremely nonlinear bulk photogalvanic currents. *Phys. Rev. Lett.* **2021**, *127*, 126601.

(27) Heide, C.; Boolakee, T.; Eckstein, T.; Hommelhoff, P. Optical current generation in graphene: Cep control vs. $\omega + 2\omega$ control. *Nanophotonics* **2021**, *0*, 20210236.

(28) Blanchet, V.; Nicole, C.; Bouchene, M.-A.; Girard, B. Temporal coherent control in two-photon transitions: From optical interferences to quantum interferences. *Phys. Rev. Lett.* **1997**, *78*, 2716–2719.

(29) Franco, I.; Brumer, P. Minimum requirements for laser-induced symmetry breaking in quantum and classical mechanics. *J. Phys. B: At., Mol. Opt. Phys.* **2008**, *41*, 074003.

(30) Wismer, M. S.; Kruchinin, S. Y.; Ciappina, M.; Stockman, M. I.; Yakovlev, V. S. Strong-Field Resonant Dynamics in Semiconductors. *Phys. Rev. Lett.* **2016**, *116*, 197401.

(31) Chizhova, L. A.; Libisch, F.; Burgdorfer, J. Nonlinear response of graphene to a few-cycle terahertz laser pulse: Role of doping and disorder. *Phys. Rev. B: Condens. Matter Mater. Phys.* **2016**, *94*, 075412.

(32) Sato, S. A.; Lucchini, M.; Volkov, M.; Schlaepfer, F.; Gallmann, L.; Keller, U.; Rubio, A. Role of intraband transitions in photocurrent generation. *Phys. Rev. B: Condens. Matter Mater. Phys.* **2018**, *98*, 035202.

(33) Shapiro, M.; Brumer, P. *Quantum control of molecular processes*; Wiley: 2012.

- (34) Gu, B.; Franco, I. Quantifying Early Time Quantum Decoherence Dynamics through Fluctuations. *J. Phys. Chem. Lett.* **2017**, *8*, 4289–4294.
- (35) Hu, W.; Gu, B.; Franco, I. Lessons on electronic decoherence in molecules from exact modeling. *J. Chem. Phys.* **2018**, *148*, 134304.
- (36) Cassette, E.; Pensack, R. D.; Mahler, B.; Scholes, G. D. Room-temperature exciton coherence and dephasing in two-dimensional nanostructures. *Nat. Commun.* **2015**, *6*, 6086.
- (37) Kraus, P. M.; Zurch, M.; Cushing, S. K.; Neumark, D. M.; Leone, S. R. The ultrafast X-ray spectroscopic revolution in chemical dynamics. *Nature Reviews Chemistry* **2018**, *2*, 82–94.
- (38) Geneaux, R.; Marroux, H. J. B.; Guggenmos, A.; Neumark, D. M.; Leone, S. R. Transient absorption spectroscopy using high harmonic generation: A review of ultrafast X-ray dynamics in molecules and solids. *Philos. Trans. R. Soc., A* **2019**, *377*, 20170463.
- (39) Heide, C.; Boolakee, T.; Higuchi, T.; Hommelhoff, P. Adiabaticity parameters for the categorization of light-matter interaction: From weak to strong driving. *Phys. Rev. A: At., Mol., Opt. Phys.* **2021**, *104*, 023103.
- (40) Sheridan, E.; Chen, L.; Li, J.; Guo, Q.; Hao, S.; Yu, M.; Eom, K.-T.; Lee, H.; Lee, J.-W.; Eom, C.-B.; Irvin, P.; Levy, J. Gate-Tunable Optical Nonlinearities and Extinction in Graphene/LaAlO₃/SrTiO₃-Nanostructures. *Nano Lett.* **2020**, *20*, 6966–6973.
- (41) Kelardeh, H. K.; Apalkov, V.; Stockman, M. I. Graphene in ultrafast and superstrong laser fields. *Phys. Rev. B: Condens. Matter Mater. Phys.* **2015**, *91*, 045439.
- (42) Li, Q. Z.; Elliott, P.; Dewhurst, J. K.; Sharma, S.; Shallcross, S. Ab initio study of ultrafast charge dynamics in graphene. *Phys. Rev. B: Condens. Matter Mater. Phys.* **2021**, *103*, L081102.
- (43) Haroche, S.; Raimond, J.-M. *Exploring the Quantum: Atoms, Cavities, and Photons*; Oxford University Press: 2006.
- (44) Heide, C.; Kobayashi, Y.; Johnson, A.; Liu, F.; Heinz, T.; Reis, D. A.; Ghimire, S. *Probing Electron-Hole Coherence in Strongly-Driven Solids*; <http://arxiv.org/abs/2109.04508> (2021) (accessed 10/14/2021).
- (45) Floss, I.; Lemell, C.; Yabana, K.; Burgdorfer, J. Incorporating decoherence into solid-state time-dependent density functional theory. *Phys. Rev. B: Condens. Matter Mater. Phys.* **2019**, *99*, 224301.
- (46) Breusing, M.; Kuehn, S.; Winzer, T.; Malić, E.; Milde, F.; Severin, N.; Rabe, J. P.; Ropers, C.; Knorr, A.; Elsaesser, T. Ultrafast nonequilibrium carrier dynamics in a single graphene layer. *Phys. Rev. B: Condens. Matter Mater. Phys.* **2011**, *83*, 153410.
- (47) Tielrooij, K. J.; Piatkowski, L.; Massicotte, M.; Woessner, A.; Ma, Q.; Lee, Y.; Myhro, K. S.; Lau, C. N.; Jarillo-Herrero, P.; Van Hulst, N. F.; Koppens, F. H.L. Generation of photovoltage in graphene on a femtosecond timescale through efficient carrier heating. *Nat. Nanotechnol.* **2015**, *10*, 437–443.
- (48) Gierz, I.; Petersen, J. C.; Mitrano, M.; Cacho, C.; Turcu, I. C. E.; Springate, E.; Stohr, A.; Kohler, A.; Starke, U.; Cavalleri, A. Snapshots of non-equilibrium Dirac carrier distributions in graphene. *Nat. Mater.* **2013**, *12*, 1119–1124.
- (49) Hahn, E. L. Spin echoes. *Phys. Rev.* **1950**, *80*, 580–594.
- (50) Kurnit, N. A.; Abella, I. D.; Hartmann, S. R. Observation of a photon echo. *Phys. Rev. Lett.* **1964**, *13*, 567–568.
- (51) Stern, A.; Aharonov, Y.; Imry, Y. Phase uncertainty and loss of interference: A general picture. *Phys. Rev. A: At., Mol., Opt. Phys.* **1990**, *41*, 3436–3448.